Artificial Neural Network (ANN) modelling of scale dependent dynamic capillary pressure effects in two-phase flow in porous media

Citation: ABIDOYE, L.K. and DAS, D.B., 2015. Artificial Neural Network (ANN) modelling of scale dependent dynamic capillary pressure effects in two-phase flow in porous media. Journal of Hydroinformatics, 17 (3), pp. 446–461.

Artificial Neural Network (ANN) Modelling of Scale Dependent Dynamic Capillary Pressure Effects in Two-Phase Flow in Porous Media

Luqman K. Abidoye, Diganta B. Das*

Chemical Engineering Department, Loughborough University, Loughborough, Leicestershire, LE11 3TU, United Kingdom

*Corresponding author (email: D.B.Das@lboro.ac.uk)

Abstract

A number of numerical simulations and experimental investigations have reported the impact of specific domain size on the dynamic capillary pressure which is one of the forces that govern two-phase flow in porous media. These investigations are often achieved with time-consuming experiments and/or costly/complex computational methods. In view of this, a computationally efficient and simple alternative platform for the prediction of the domain scale dependence of the dynamic capillary pressure effects, defined in terms of a coefficient named as dynamic coefficient (τ), is developed using artificial neural network (ANN). The input parameters consist of the phase saturation, media permeability, capillary entry pressure, viscosity ratio, density ratio, temperature, pore size distribution index, porosity and domain volume with corresponding output τ obtained at different domain scales. Good generalization of the model was achieved by acquiring data from independent sources comprising experiments and numerical simulations. Different ANN configurations as well as linear and non-linear multivariate regression models were tested using a number of performance criteria. Findings in this work showed that the ANN structures with two hidden layers perform better than those with single hidden layer. In particular, the ANN configuration with 13 and 15 neurons in the first and second hidden layers, respectively, performed the best. Using this best-performing ANN, effects of increased domain size were predicted for three separate experimental results obtained from literature and our laboratory with different domain scales. Results showed increased magnitude of τ as the domain size increases for all the independent experimental data considered. This work shows the applicability and techniques of using ANN in the prediction of scale dependence of two-phase flow parameters.

Keywords: Multi-scale, dynamic capillary pressure effects, dynamic coefficient, ANN, two-phase flow, viscosity ratio, porous media

1. Introduction

Characterising single and two-phase flow in porous media is of particular interests in issues relating to remediation of contaminant, oil recovery, flow in pulp and paper systems, geological sequestration of CO_2, and others (Das et al. 2014; Abidoye et al. 2014; Bear 2013; Kobayashi et al. 2008; Hill et al. 2007; Ingham and Pop 2005). The topic of the paper, namely, the two-phase flow behaviour in porous medium can be macroscopically described by the equations for conservations of fluids' mass and momentum (Kalaydjian 1987); however, these should be coupled with constitutive relationships among capillary pressure, (P^c), saturation (S) and relative permeability (K_r) (Abidoye et al. 2014; Khudaida and Das, 2014). The traditional approaches for determining the P^c-S-K_r relationships assume that the flow parameters are functions of steady-state saturation, i.e., when dS/dt = 0. For example, the definition of P^c according to the Laplace law ($P^c = \frac{2\gamma \cos\theta}{r}$) is valid under static conditions (Kalaydjian 1992) where γ is the interfacial tension between the two fluids and θ is the contact angle. As evident, the law defines P^c to be a function of contact angle (θ) which, in turn, depends on the physical properties of the fluids and the porous medium (e.g., wettability (Dullien et al. 1990) and viscosity ratio (Danish and Jacquin 1983)) that are in contact with one another. Despite these notions, the saturation-rate (dS/dt) dependency of the P^c-S relationships has been observed in many studies during dynamic two-phase flow in porous media which is referred to as the dynamic capillary pressure effect (Hassanizadeh et al. 2002; Mirzaei and Das, 2006).

A large number of papers involving numerical simulations and experiments concerning the dynamic P^c-S relationship have been published (see e.g., Topp et al. 1967; Smiles et al. 1971; Stauffer 1978; Kalaydjian 1992; Wildenschild et al. 2001; Hassanizadeh et al. 2002; Denis M O'Carroll et al. 2005; D M O'Carroll et al. 2005; Oung et al. 2005; Camps-Roach et al. 2010; Sakaki et al. 2010; Goel and O'Carroll 2011; Das and Mirzaei 2012; Diamantopoulos and Durner 2012; Das and Mirzaei 2013; Khudaida and Das, 2014). Particularly, the studies by Kalaydjian (1992) and, Hassanizadeh and Gray (1993) identified the dependence of the P^c on saturation (S) and the rate of change of saturation $\left(\frac{\partial S}{\partial t}\right)$. This is defined as 'dynamic capillary pressure effect' and it is quantitatively described by a proportionality constant term, τ, known as the dynamic coefficient. In the last couple of decades, attempts have been to incorporate this term in the traditional mathematical definition for the two-phase systems as expressed in equation (1) to account for the difference in the P^c-S relationships under the dynamic and static flow conditions:

$$P^{c,dyn} - P^{c,static} = -\tau\left(\frac{\partial S}{\partial t}\right) \quad (1)$$

where, $P^{c,dyn}$ [$kg \cdot m^{-1} \cdot s^{-2}$] is the phase pressure difference (P_{nw}-P_w) measured under dynamic or non-equilibrium condition, $P^{c,static}$ [$kg \cdot m^{-1} \cdot s^{-2}$] is the capillary pressure measured under equilibrium condition, $\frac{\partial S}{\partial t}$ [s^{-1}] is the rate of saturation change, and τ [$kg \cdot m^{-1} \cdot s^{-1}$] is the dynamic coefficient as mentioned earlier. P_w and P_{nw} are the pressures of the wetting and non-wetting phases, respectively at the interface between the two phases.

As explained by Das et al. (2007), the magnitude of τ relates to how close or far from capillary equilibrium ($\frac{\partial S}{\partial t}=0$) is the two-phase flow system. However, its magnitude is reported to be dependent on the size of the domain (Dahle et al. 2005; Camps-Roach et al. 2010; Bottero, Hassanizadeh and Kleingeld 2011; Bottero et al. 2011; Das and Mirzaei 2012; Das and Mirzaei 2013) apart from other factors, e.g., fluid viscosity and density ratios (Gielen et al. 2005; Das et al. 2007; Goel and O'Carroll 2011; Joekar-Niasar and Majid Hassanizadeh 2011), permeability of the medium (Camps-Roach et al. 2010; Tian et al. 2012; Hanspal et al. 2013) and heterogeneities (Das et al. 2006; Manthey et al. 2005; Das and Mirzaei 2013; Mirzaei and Das, 2013). This paper is specifically concerned with the domain scale effects on the dynamic coefficient (τ) as discussed below.

Understanding the influence of domain scale on the magnitude of τ is important as the two-phase flow can occur in porous domains at pore, core and/or larger field scales. Previous experimental (Bottero et al. 2011b) and numerical (Dahle et al. 2005) studies showed an increasing magnitude of τ as the domain size increases. However, some authors have expressed different conclusions about the effect of domain size on τ. Camps-Roach et al. (2010) and Das and Mirzaei (2012, 2013) do not find significant difference between the locally measured and the upscaled value of τ. This indicates the possible inconsistency surrounding the exact trend of the magnitude of τ with the domain scale.

Meanwhile, investigating the dynamic capillary pressure effects on two-phase flow systems in the porous media often requires time-consuming experiments and/or cost-intensive modelling and simulations, which generally involve complex procedures to set up and run the simulations (Hanspal et al. 2013; Spalding 1981; Khudaida and Das, 2014). Furthermore, determining the effects of domain scale on τ also impose further challenges with the implications of various averaging techniques which are proposed and applied in the literature. For example, Bottero et al. (2011a) proposed centroid-corrected averaging method as the most appropriate for two phase system while authors such as Das and Mirzaei (2012, 2013), Camps-Roach et al. (2010) and Manthey et al. (2005) employed different averaging techniques to determine the scale dependency of τ. While the scale dependency of τ continues to be a topic of discussion, there is an obvious lack of industrially relevant, easy to use, tools that can easily determine these behaviour. To address these

challenges/issues, we wish to investigate the domain scale effect on τ using alternative platforms offering less complex and fast implementation procedures to achieve the same end. As such, a computationally economical and simpler platform for investigating the effects of domain scale on τ is presented using artificial neural network (ANN).

Indeed, ANN is a powerful modelling tool with the ability to learn and generalize functions from rounds of training as well as extract essential information from data (Khashei and Bijari 2013; Wang and Fu 2008). It provides a novel, elegant and valuable class of computational tools for data analysis and prediction (Deka and Quddus 2014; White, 1989). Its building blocks or the elements are the 'neurons' which are grouped into input, hidden and output layers with respective biases, weights and transfer functions (Yurdakul and Akdas 2013; Mueller and Hemond 2013). The network manipulates the values of the biases and weights in a sequence of training processes and uses the transfer functions to establish the relationships between the inputs and the outputs. It has found applications in wide areas of science and engineering problems including medical fields to illustrate medical diagnosis (Amato et al. 2013), renewable energy systems, economics, psychology and many more (Kalogirou 2013).

Although the modelling parameters involved in the two-phase flow in porous media are interrelated in a complex manner, it has been shown that ANN can approximate the relevant functions to the desired accuracy (Zhang et al. 1998; Hanspal et al., 2013). This quality of ANN can, thus, be harnessed to investigate the complex behaviour of two-phase flow in porous media. For example, please see the works on the application of ANN to study two-phase flow pattern (Mehta et al. 2013), oil flow rate (Ahmadi et al. 2013), groundwater contamination and pollutant infiltration forecasting (Tabach et al. 2007), optimization of groundwater remediation problems (Rogers and Dowla 1994; Johnson and Rogers 2000), large-scale water resource management (Yan and Minsker 2006; Mounce et al. 2013), and permeability modelling in petroleum reservoir management (Karimpouli et al. 2010). Recently, Hanspal et al. (2013) demonstrated the effectiveness of ANN in the determination of dynamic effects in two-phase flow system, though they did not investigate the effect of domain scale on τ. They concluded that a well-trained and validated ANN structure can give reliable prediction of τ in two-phase flow system. In addition to being inexpensive, ANN offers a faster alternative to modelling of complex system with the freedom from excessive imposition of constraints on the complex relationships between the input and output variables. Thus, our work explores the above qualities of ANN to investigate the domain scale dependency of τ in the two-phase flow system in porous media.

2 Modelling approaches

ANN and multivariate regression (MVR) techniques were used to investigate the domain scale dependency of the τ in the two-phase flow system. The MVR was chosen because of the ease of implementation and to provide an alternative approach to compare different ANN configurations against.

2.1 ANN

For successful modelling of dynamic two-phase flow behaviour using ANN, the impacts of the network configuration, training and evaluation procedures cannot be overemphasised. In this work, different network configurations were investigated using a feed forward network. This is the commonest network in engineering application (Kalogirou 2013; Deka and Quddus, 2014). For the purpose of training, back-propagation algorithm was employed. Details of the configurations, training and data processing are discussed below.

2.1.1 Data sources and pre-processing

In this paper, the literature data were obtained from the results by Das and Mirzaei (2012), Hanspal and Das (2012), Goel and O'Carroll (2011), Das et al. (2007), Mirzaei and Das (2007) and additional data (Abidoye and Das 2014) from in-house laboratory experiments using methodology described by Das and Mirzaei (2012). Nine independent variables that have been identified as important in the literature were used as input variables in the simulations. These include, water saturation (S), media permeability (k), capillary entry pressure (P_d), fluid viscosity ratio (μ_r) defined as the ratio of the non-wetting phase viscosity (μ_{nw}) to that of the wetting phase viscosity (μ_w), fluid density ratio (D_r) defined as the ratio of the non-wetting phase density (D_{nw}) to that of the wetting phase density (D_w), temperature (T), pore size distribution index (λ), porosity (ϕ), and domain volume (V). The output variable is the corresponding τ. The number of data points under each variable is 307. In selecting these data sources, efforts were made to ensure that the data contain varying experimental or simulation parameters and conditions needed to fulfil the objective of this paper. For example, the works of Das and Mirzaei (2012), Goel and O'Carroll (2011), Mirzaei and Das (2007) and, Hanspal and Das (2012) were conducted using different domain volumes. Furthermore, our laboratory experiments (Abidoye and Das 2014) were conducted for different heights of domain (4, 8 and 12 cm height) but with the same diameter for 500 cSt viscosity ratio of silicone-oil water system. These features enhance the training of the ANN network to easily capture the non-linear relationships between the domain size and τ. Important statistics of the variables are listed in Table 1.

Compared to the number of data points commonly required to plot a complete τ-S curve (typically less than 10 data points, see, e.g., Bottero et al. (2011b)), the amount of data used in this work (>300 data points) is over 30 times more than what is typically required. Also, this work employs simple ANN structure. These features ensure that artificial over-fitting of the data is avoided. Complex ANN structures and few data can lead to artificial over-fitting in ANN modelling (Hanspal et al. 2013).

2.1.2 ANN development

Various configurations of ANN were developed and tested to determine he most suitable network. The configuration approach followed that demonstrated in Hanspal et al. (2013) as proposed by

Srinivasulu and Jain (2006). The ANNs include single and double hidden layers. Program file with lines of code was written and implemented in MATLAB to create, train, validate and test the networks as well as to generate the goodness of fit of the parameters e.g. correlation coefficients and slope for the predicted output (τ). The developed networks consist of different layers comprising the input, hidden and the output layers. The input layer is occupied by the independent variables while the output layer is for the dependent variable. The hidden layer is occupied by the neurons which are the constitutive units that receive the input and operate on them to produce the output. The code divides the dataset randomly into 60, 20 and 20% corresponding to the data for training, validation and testing. As stated before, the training was performed with Levenberg-Marquardt function (Marquardt 1963) using back-propagation algorithm. Levenberg-Marquardt function is a curve-fitting function applied in the non-linear least squares problems. It optimises the parameter of the model curve by minimising the sum of the squares of the deviation from the empirical dependent variable. The back-propagation learning algorithm operates by iterative adjustment of the weights and biases in response to the error value between the predicted and the desired outputs. 'Tansig' and 'Purelin' transfer functions were used in this work. These transfer functions calculate a layer's output from its net input. While 'Tansig' is nonlinear, 'Purelin' is linear. For a network with single hidden layer, 'Tansig' was used between the input and the hidden layers while 'Purelin' was used between the hidden and the output layer. For a network with double hidden layer, 'Tansig' was used between the input and the hidden layers as well as between the first to the second hidden layers while 'Purelin' was used between the second hidden layer and the output.

Mean square error (MSE) was employed as the network default performance criterion relating the calculated outputs from the ANN to the actual target (dependent variable) in the training, validation and testing processes. In the simulation, pre-processing was performed using lines of code in the script with function "mapminmax". This function scales the inputs so that they fall into the range of -1 to 1.

In the training process, the epochs and goals serve as the stopping criteria of the number of iterations and the error tolerance, respectively. Epoch is the maximum number of times all of the training sets presented to the network while goal refers to the maximum error tolerance to be met by the developed network. Thus, the training stops if the error goal is met or the maximum number of epochs is attained. In this work, an epoch of 200 and a goal of zero were used. Different network configurations were constructed and each configuration differs in the number of hidden layers or neurons. The number of neurons was gradually increased for either single or two-hidden layers. In this work, the representation of the layers in the ANN configurations is ANN [X-H1-Y] and ANN [X-H1-H2-Y] for single and double hidden layers, respectively. "X" represents the input layer and its number refers to the number of independent variables, "H1" and "H2" represent the first and the second hidden layers, respectively and their number represent the number of neurons in that layer. "Y" is the output layer and its number represents the number of the dependent variable.

Table 1: Statistics of the input and output variables

	Water saturation, S (-)	Permeability, k (m^2)	Entry pressure, P_d (Pa)	Domain volume, V (m^3)	Pore size distribution, λ (-)	Viscosity ratio, μ_r (-)	Porosity, ϕ (-)	Density ratio, D_r (-)	Temperature, T (^oC)	Dynamic coefficient, τ (Pa.s)
Maximum	$9.96x10^{-1}$	$5.00x10^{-9}$	$1.50x10^{3}$	$1.57x10^{-3}$	8.84	$1.00\ x10^{3}$	0.400	2.00	80.00	$1.05\ x10^{11}$
Minimum	$1.05x10^{-1}$	$1.50\ x10^{-11}$	$3.75x10^{2}$	$3.27\ x10^{-4}$	2.07	$5.00\ x10^{-1}$	0.32	0.50	20.00	$1.18\ x10^{3}$
Arithmetic Average	$4.78x10^{-1}$	$1.70\ x10^{-9}$	$7.78x10^{2}$	$9.41\ x10^{-4}$	3.44	$1.77\ x10^{2}$	0.373	1.15	22.4	$5.57\ x10^{9}$
Standard deviation	$2.57x10^{-1}$	$2.19\ x10^{-9}$	$4.29x10^{2}$	$2.42\ x10^{-4}$	1.49	$2.66\ x10^{2}$	0.0311	0.374	9.43	$1.89\ x10^{10}$

2.2 Linear (LR) and non-linear (NLR) regression models

For the purpose of comparisons with the performances of the different ANN configurations, multiple linear (LR) and non-linear (NLR) regression models were investigated with the aid of MATLAB. Both regression models utilised the entire dataset.

TheLR was formulated for the nine independent variables against the dependent variable, τ as shown in equation (2):

$$\tau = b_0 + b_1(\chi_1) + b_2(\chi_2) + b_3(\chi_3) + b_4(\chi_4) + b_5(\chi_5) + b_6(\chi_6) + b_7(\chi_7) + b_8(\chi_8) + b_9(\chi_9) \quad (2)$$

b_o,...., b_9 are the regression coefficients, χ_1,....,χ_9 represent the independent variables. The regression coefficients for the LR were determined using the left division method (Gauss elimination and least square techniques) (Hanspal et al. 2013).

For the non-linear regression of the independent variables, polynomials of various orders (Jain and Indurthy 2003) were used. The regression was implemented using non-linear fitting function (nlfit) in MATLAB to determine the vector of fit coefficients (b_o,...., b_9) in the models listed below:

$$\tau = b_0 + b_1(\chi_1)^{0.05} + b_2(\chi_2)^{0.05} + b_3(\chi_3)^{0.05} + b_4(\chi_4)^{0.05} + b_5(\chi_5)^{0.05} + b_6(\chi_6)^{0.05} + b_7(\chi_7)^{0.05} + b_8(\chi_8)^{0.05} + b_9(\chi_9)^{0.05} \quad (3)$$

$$\tau = b_0 + b_1(\chi_1)^2 + b_2(\chi_2)^2 + b_3(\chi_3)^2 + b_4(\chi_4)^2 + b_5(\chi_5)^2 + b_6(\chi_6)^2 + b_7(\chi_7)^2 + b_8(\chi_8)^2 + b_9(\chi_9)^2 \quad (4)$$

$$\tau = b_0 + b_1(\chi_1)^3 + b_2(\chi_2)^3 + b_3(\chi_3)^3 + b_4(\chi_4)^3 + b_5(\chi_5)^3 + b_6(\chi_6)^3 + b_7(\chi_7)^3 + b_8(\chi_8)^3 + b_9(\chi_9)^3 \quad (5)$$

$$\tau = b_0 + b_1(\chi_1)^4 + b_2(\chi_2)^4 + b_3(\chi_3)^4 + b_4(\chi_4)^4 + b_5(\chi_5)^4 + b_6(\chi_6)^4 + b_7(\chi_7)^4 + b_8(\chi_8)^4 + b_9(\chi_9)^4 \quad (6)$$

2.3 ANN performance testing criteria

The performance of all ANNs were weighed with different statistical evaluations as demonstrated in Hanspal et al. (2013) using the following statistical analyses:

A. Sum square error (SSE)

This describes the total deviation of the predicted values (S_{cal}) from the target values (S_{obs}):

$$SSE = \sum_{i=1}^{N} \left(S_{obs} - S_{cal}\right)^2 \quad (7)$$

Where N = Total number of data points predicted, S_{obs}= observed or target values of dynamic coefficient, τ and S_{cal} = predicted or calculated value of dynamic coefficient, τ .

B. Average absolute relative error (AARE)

This is the average of the relative errors in the prediction of a particular variable and it is expressed as a percentage. Lower values of AARE indicate better model performance. It can be computed as follows:

$$AARE = \frac{1}{N} \sum_{i=1}^{N} \left| \frac{S_{cal} - S_{obs}}{S_{obs}} \right| \times 100 \quad (8)$$

C. Nash-Sutcliffe efficiency coefficient (E)

The Nash-Sutcliffe efficiency coefficient is used to describe the accuracy of model outputs in relation to observed data. A value of E equal to 1 depicts a perfect match between observed data and outputs therefore the closer the model efficiency is to unity the more accurate the model. E is computed as follows:

$$E = 1 - \frac{\sum \left(S_{cal} - S_{obs}\right)^2}{\sum \left(S_{obs} - \overline{S}_{obs}\right)^2} \quad (9)$$

Where $\overline{S}_{obs}$ = average observed dynamic coefficient, τ , in this work.

D. Pearson product moment coefficient of correlation (R)

This is a measure of the strength of linear dependence in the relationship between calculated and observed values of a modelled variable. Values of R equal to 1.0 indicate a perfect model. It is computed as follows:

$$R = \frac{\sum \left(S_{obs} - \overline{S}_{obs}\right) \times \left(S_{cal} - \overline{S}_{cal}\right)}{\sqrt{\sum \left(S_{obs} - S_{obs}\right)^2 \sum \left(S_{cal} - \overline{S}_{cal}\right)^2}} \quad (10)$$

Where $\overline{S}_{cal}$ = average calculated dynamic coefficient, τ , in this work.

E. Threshold statistics (TS)

The threshold statistic for a level of absolute relative error of $x\%$ from a particular model is a measure of consistency in the prediction errors (Jain and Ormsbee, 2002). The threshold statistic can be computed as follows:

$$TS = \frac{N_x}{N} \tag{11}$$

Where N_x = number of data points predicted for which the average relative error (ARE) is less than $x\%$. Larger values of threshold statistics indicate better model performance.

F. Mean squared errors (MSE)

Mean squared error measures the average of the squares of the errors between the observed value (S_{obs}) and the predicted or estimated value (S_{cal}). In N, number of data points or cases. MSE can be obtained by averaging the SSE (see equation 7)

$$MSE = \frac{1}{N}\sum_{i=1}^{N}\left(S_{obs} - S_{cal}\right)^2 \tag{12}$$

2.4 Prediction of domain scale dependency of τ-S relationships

Following the rigorous statistical evaluation of the models developed and described above, prediction of the effect of domain size on the τ-S relationships was performed using the best-performing model. Separate data from independent experiments are predicted separately. To do this, the actual domain volume (V) of the experiment was increased by 10 or 20% and the corresponding τ was predicted as a function of saturation using the best-performing ANN.

3 Results and discussions

A computationally cost-effective and reliable ANN structure that predicts the domain scale dependency of τ-S relationships will serve useful purpose in determining the significance of dynamic capillary pressure for two-phase flow systems. Our results aim to demonstrate this possibility. So, the results of training, validation and testing of the ANNs are discussed below. Also, the performances of the different ANN configurations together with the MVR models are compared on the bases of the different performance criteria. Scale dependency of τ-S relationships were then predicted for two-phase flow system using the best-performing configuration.

3.1 ANN configurations

The training, validation and testing as well as the post-training regression analyses for different ANN configurations are shown in Figures 1 and 2 for ANN [9-13-15-1] and ANN [9-15-17-1], respectively. Figure 1(A) shows how the mean squared error (MSE) reduces during training, validation and testing as the number of epoch increases. This eventually culminates in the optimal performance during validation at 108 epochs having approximately zero MSE value, i.e., 0.0023. This behaviour shows that the network learns well as the number of epochs increase. The testing session shows acceptable MSE that is very close to zero as well. The post-training regression analysis (Figure 1(B)) shows the linear regression line fit the data points. This regression line has a correlation coefficient (c) and slope (m) of 0.99 and 0.97, respectively, which are very close to 1. These show the reliability of the fit. In the figure, it can be observed that the target data cluster around the regression line in a way that shows reliable prediction. Similarly, the behaviour of the network for ANN [9-15-17-1] is shown in Figure 2. The network exhibits similar behaviour as discussed above. The learning improves with the number of epochs for the training, validation and testing (Figure 2(A)). This is indicated by the reduction in the MSE values and the optimal MSE with validation occurs before the number of epochs reaches 51. In comparison to the behaviour of ANN [9-13-15-1], shown in Figure 1(A), the testing and validation errors are larger in Figure 2(A), under corresponding condition. The regression line for the ANN structure [9-15-17-1] is shown in Figure 2(B). The fit shows good c and m values of approximately 0.95 and 1.00, respectively. The regression analysis in Figure 2(B) shows that the cluster of the target data around the regression fit line is more scattered unlike that shown for ANN [9-13-15-1] (Figure 1(B)). This gives indication that ANN [9-13-15-1] may be more reliable than ANN [9-15-17-1]. However, the latter learns faster than the former.

The performances of various ANN configurations, in terms of the values of c and m of the regression line of fits to the target data τ are listed in Table 2. As well known, values of the slope, m and correlation coefficient, c, closer to 1 indicate reliable prediction. From the table, it can be observed that majority of the ANN configurations perform well as indicated by the high values of the c and m. However, the two-hidden-layer models perform better than the single-hidden-layer models as they have the slope and correlation coefficient closer to 1 than the single-hidden-layer structure. In all, ANN [9-13-15-1] and ANN [9-15-17-1] appear to be leading in performance. However, the criteria listed in subsection 2.3 are further employed in weighing the performance of all the models including the MVR models. In Table 2, the slope of the regression line obtained from ANN [9-15-17-1] is shown to be slightly greater than 1 (i.e., 1.02). This can be explained to mean slight over prediction of the target data by the

312 model. This is also visible in the Figure 2(B) where the line of fit is slightly above the best line
313 of fit (i.e., Y=T). In contrast, Figure 1 shows that the regression line obtained from ANN [9-
314 13-15-1] lies slightly below the best line of fit (i.e., Y=T) and hence, the slope is slightly
315 below 1 (i.e., 0.97).

316

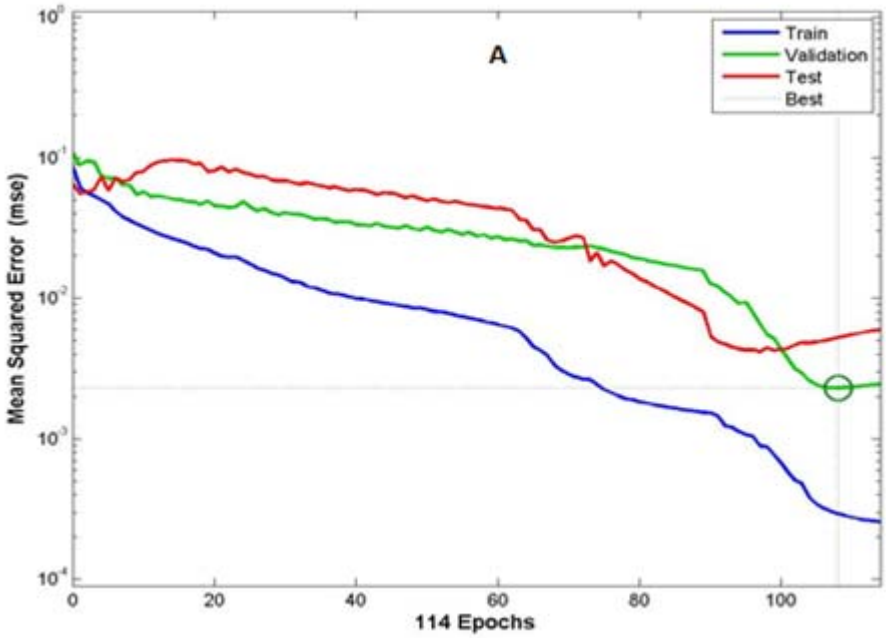

317

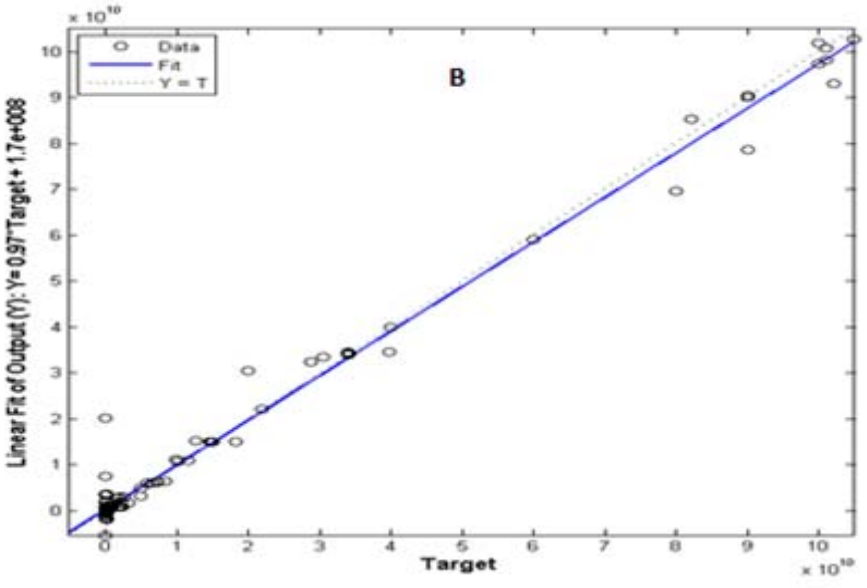

318

319 Figure 1: (A) Training and (B) post-training regression analysis using ANN [9-13-15-1]

320

321

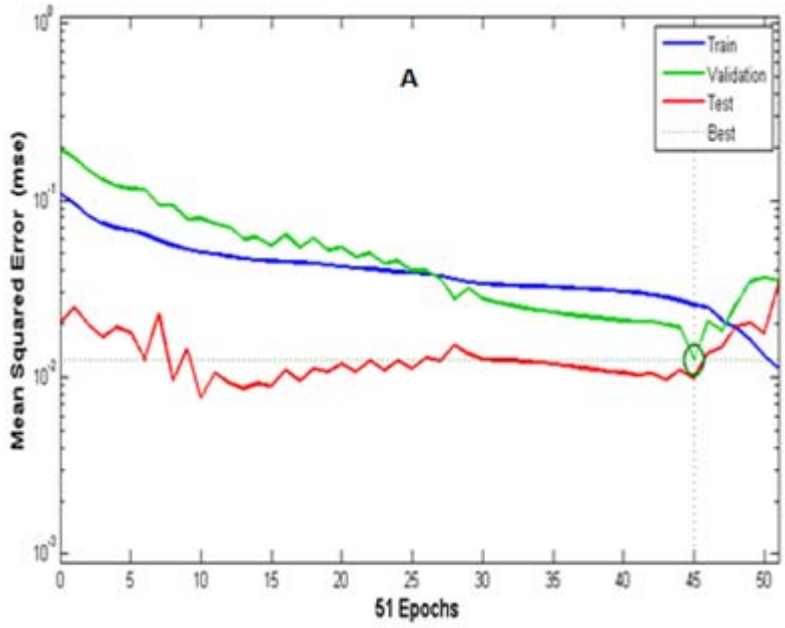

322

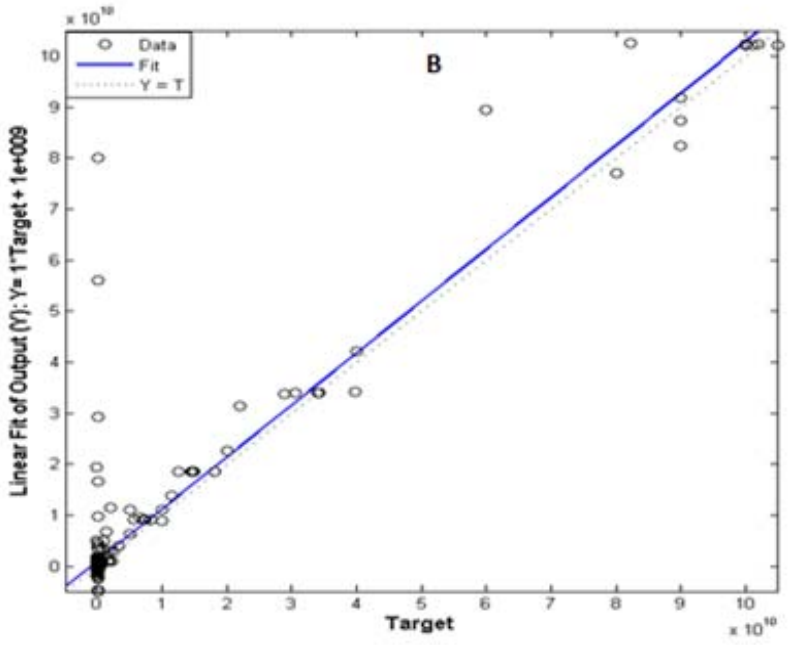

323

324 Figure 2: (A) Training and (B) post-training regression analysis using ANN [9-15-17-1]

325

Table 2: Slope and correlation coefficient for different ANN configurations (single and double hidden layered ANN structures)

S/N	ANN Configurations	Slope (m)	Correlation Coefficient (c)
1	9-2-1	0.7986	0.7986
2	9-3-1	0.8557	0.8557
3	9-4-1	0.925	0.925
4	9-5-1	0.8819	0.8819
5	9-7-1	0.8459	0.8459
6	9-9-1	0.9218	0.9218
7	9-10-1	0.8976	0.8976
8	9-2-2-1	0.881	0.881
9	9-3-2-1	0.8345	0.8345
10	9-2-3-1	0.8962	0.8962
11	9-5-3-1	0.9191	0.9191
12	9-7-5-1	0.9406	0.9406
13	9-9-7-1	0.9262	0.9262
14	9-10-8-1	0.9529	0.9529
15	9-10-10-1	0.9631	0.9631
16	9-11-13-1	0.9865	0.9865
17	9-13-15-1	0.9723	0.9949
18	9-15-17-1	1.0185	0.9468

Figure 3 shows the plots of average absolute relative error (AARE) for all ANN configurations, linear regression (LR) and non-linear regression (NLR) models. In comparison, AARE is generally low for the different ANN configurations while the LR and NLR generally have high AARE. The lower the AARE the better the performance (Hanspal et al. 2013). Thus, it seems that the ANNs perform better than the LR and NLR models. Among the ANN configurations, ANN [9-13-15-1] has the least AARE followed by ANN [9-11-13-1].

In Figure 4, the plots of the sum squared error (SSE) similarly show that the SSE is generally higher for LR and NLR models. For the ANN structures, the ANN [9-13-15-1] configuration has the least SSE followed by ANN [9-11-13-1]. Comparison of the model output in relation to the target is described in term of Nash-Sutcliffe efficiency coefficient (E) depicted in Figure 5 for all the models. Again, it is visible that ANN [9-13-15-1] has the highest efficiency followed by ANN [9-11-13-1]. Also, threshold statistics (TS) for all the models show that ANN

[9-13-15-1], ANN [9-11-13-1] and ANN [9-15-17-1] have the leading percentages. The plots are shown in Figure 6 for TS 5, TS 10, TS 25, TS 50 and TS 100. High values of TS imply good model performance.

From the above discussions, the performance criteria show that ANN structures have better reliability in predicting the two-phase flow parameters than MVR models (both linear and non-linear). From the results, ANN [9-13-15-1] has shown the best performance.

3.2 Prediction of τ-S relationships

Results of the statistical analyses discussed in section 3.1 compare the predicted output of the models to the actual target output (τ). The discussions in this section focus on the comparison of the actual τ-S relationships (target) to that predicted by some selected ANN, which include the best-performing model: ANN [9-13-15-1]. Figure 7 shows the plot of τ-S relationships using the entire dataset in comparison with the prediction by ANN [9-13-15-1]. One can observe that the ANN structure has a good predictive ability of the τ-S relationships at both low and high saturation. Almost the entire τ-S dataset are overlaid by the predicted values. In the figure, τ is shown to increase as the saturation reduces. From the start of the displacement of the wetting phase by the non-wetting phase, there exists only minimal change in τ as the saturation reduces. The trend, however, changes around the irreducible saturation where the τ value rises very steeply. This trend is widely reported in literature (Das and Mirzaei 2013; Goel and O'Carroll 2011; Camps-Roach et al. 2010; Sakaki et al. 2010). According to Das et al. (2007), increase in the magnitude of τ indicates increased deviation of the P^c-S relationships from equilibrium condition. Since the magnitude of τ becomes spectacularly large towards irreducible saturation, one can infer that the system properties at this region exhibit wider deviations from equilibrium.

Predictions of the τ-S relationships by ANN [9-15-17-1], ANN [9-10-10-1] and ANN [9-11-13-1] are shown in Figures 8, 9 and 10, respectively. While these plots show good prediction of the τ-S relationships for the entire dataset, they show more mismatches in comparison with Figure 7, especially at low water saturation or at high values of τ. However, ANN [9-11-13-1] and ANN [9-10-10-1] appear to predict better than ANN [9-15-17-1], having lower number of mismatches especially at low water saturation.

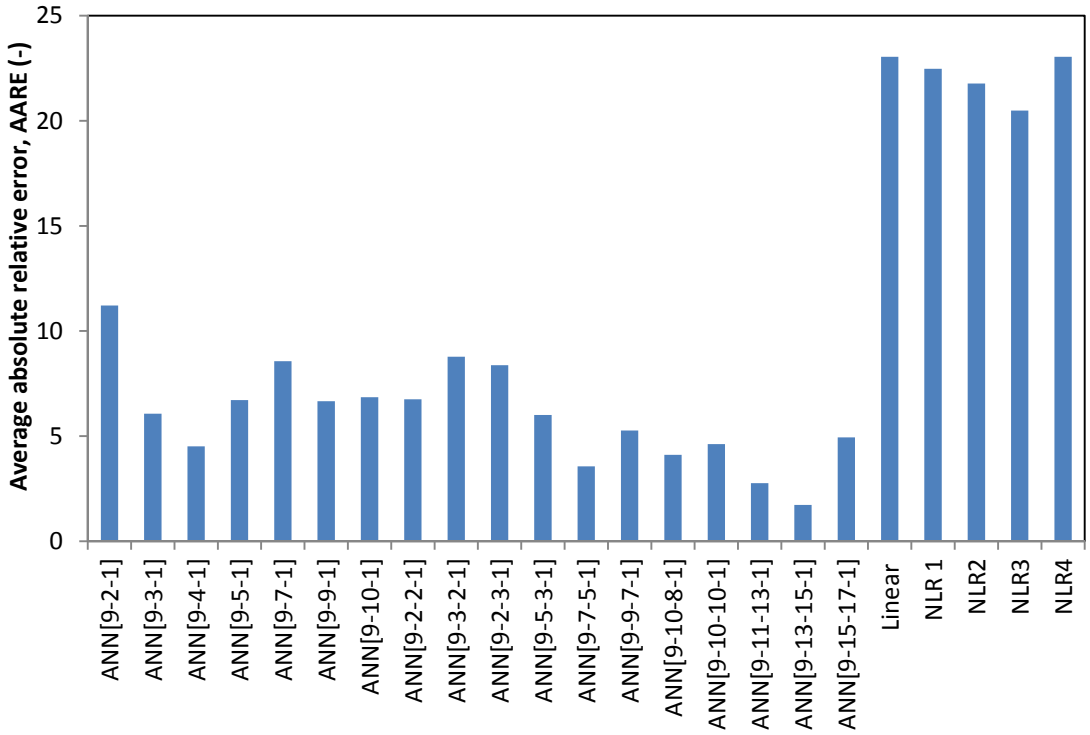

370

371 Figure 3: Average absolute relative error (AARE) for ANN, linear (LR) and non-linear (NLR)
372 regression models.

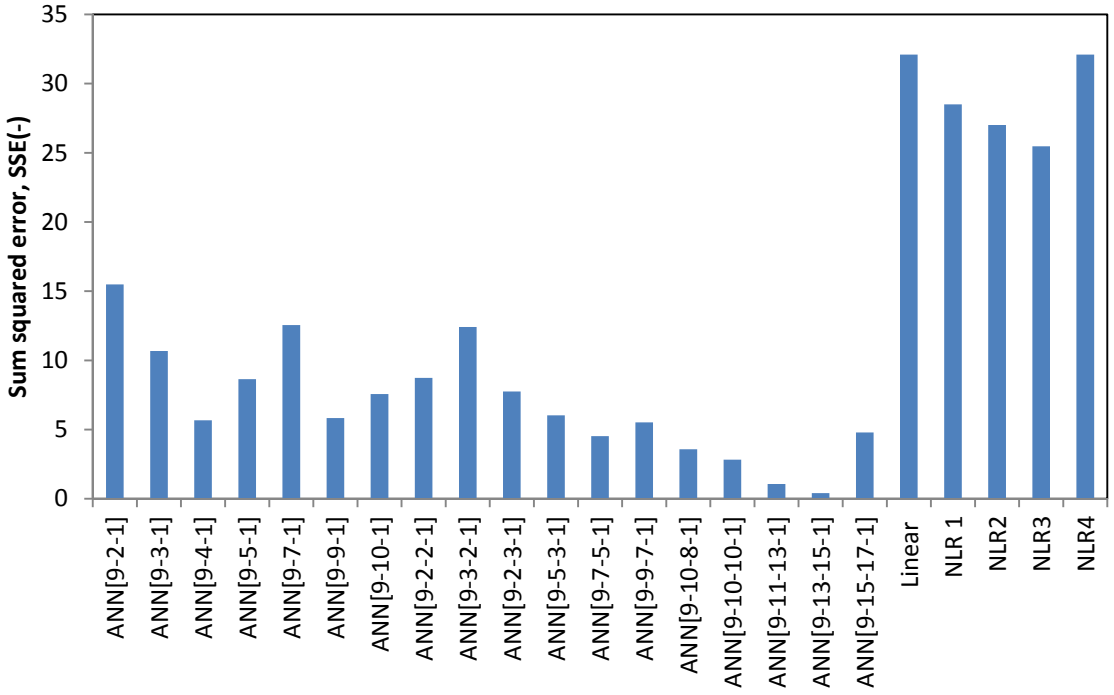

373

374 Figure 4: Sum squared error (SSE) for ANN, linear (LR) and non-linear (NLR) regression
375 models.

376

377

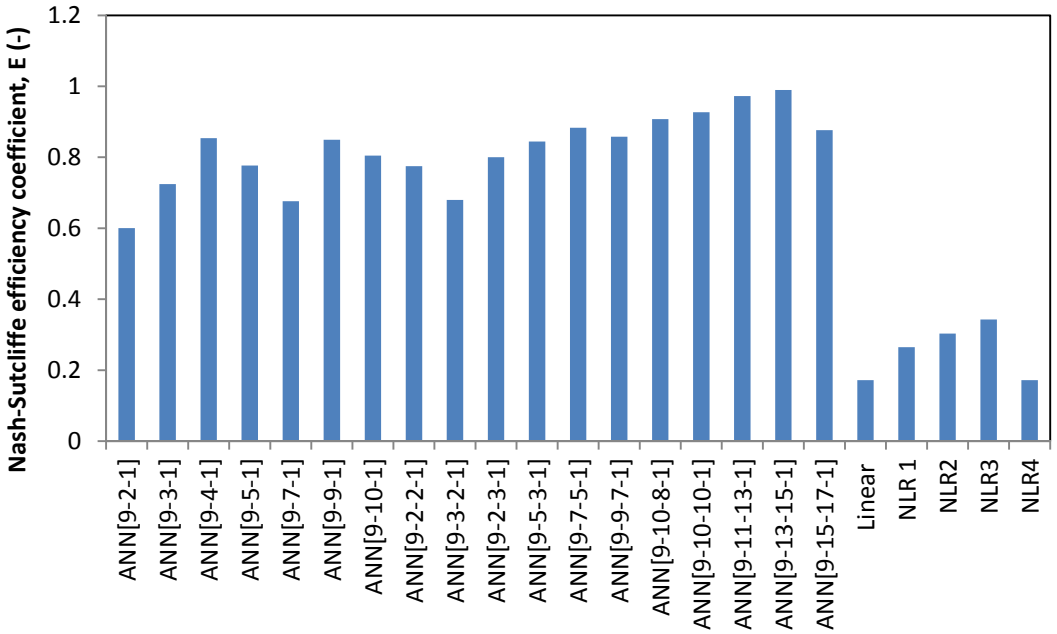

378

379 Figure 5: Model output efficiency for ANN, linear (LR) and non-linear (NLR) regression
380 models.

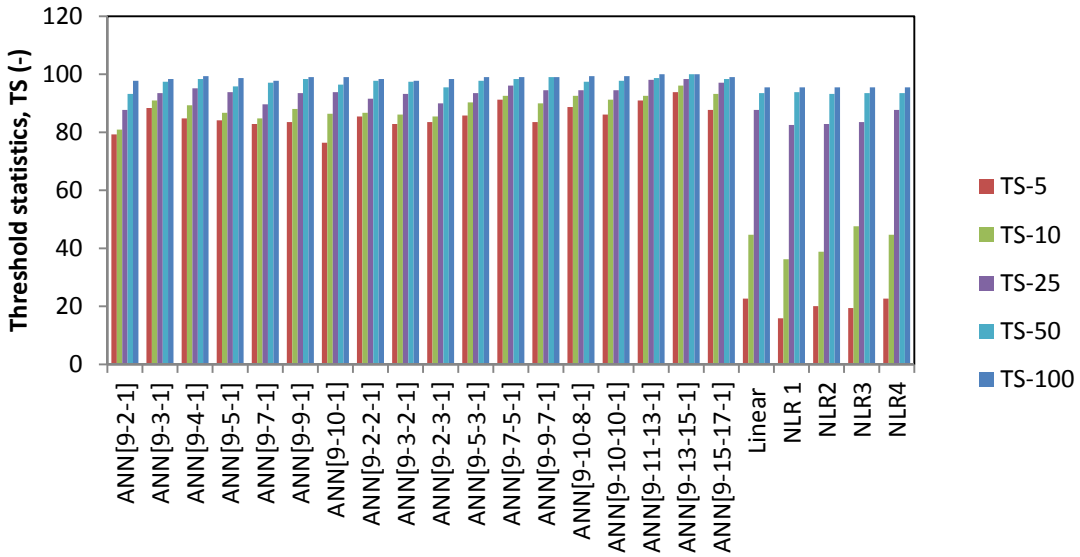

381

382 Figure 6: Threshold statistics (TS) for ANN, linear (LR) and non-linear (NLR) regression
383 models.

384 Plots of the predictions of τ-S relationships by linear and non-linear regression models are
385 shown in Figures 11 and 12. The predictions by these models are less reliable, especially at
386 low water saturation where the τ values are higher. Even the performances of these
387 regression models are much less-satisfactory in comparison to any of the ANN

388 configurations with plots shown in Figures 7 to 10. This reveals the limitations of the
389 regression models in the prediction of τ-S relationships for two-phase flow systems.

390 Judging from the results of the statistical analyses on the prediction of τ as well as the
391 above models performances on the prediction of τ-S relationships, one can conclude that
392 ANN [9-13-15-1] is the best structure among the models tested in this work. This conclusion
393 is similar to that of Hanspal et al. (2013). They found that the regression models performed
394 poorly in the prediction of the τ-S relationships and concluded that generally the regression
395 models are much less in predictive ability than ANN structures for two-phase flow system
396 characteristics. In their work, the display of non-linear regression models seem better than
397 shown in Figure 12 of this work even though similar functions were used. This can be
398 explained by the fact that they utilise only five independent variables in their work as different
399 from nine used in this work. Therefore, one can infer that the performance of the regression
400 models becomes less reliable as the number of independent variables increases for two-
401 phase flow system.

402 **3.3 Domain scale dependency of τ-s relationships**

403 In the previous analyses and discussions, the ANN [9-13-15-1] structure is shown to be the
404 best-performing network in the context of this work. In this section, the network is used to
405 predict the domain scale dependency of τ-S relationships on the basis that the network is
406 trained and validated. Separate data from different experiments are independently predicted.
407 These include data from the literature as well as our in-house laboratory experiments.

408 Figures 13-15 display the results of the predictions. In the figures, τ for the original domain
409 size is represented by two plots. One plot was obtained from the experimental data and the
410 other was obtained from the ANN prediction of the original experimental data at the original
411 domain scale (volume). These are labelled original volume (experiment) and the original
412 volume (ANN) for the actual experimental data and the ANN prediction, respectively. The
413 other two plots in each of the figures are obtained when the domain scale (volume) is
414 increased by 10 and 20%, respectively, and the corresponding τ-S relationships are
415 predicted using ANN [9-13-15-1]. The results show that increasing the volume of the domain
416 increases the magnitude of τ. This is shown in Figure 13. At 10% increase in original
417 domain volume, τ-S curve lies higher than at the original domain size. This effect becomes
418 greater at 20% increase in domain volume.

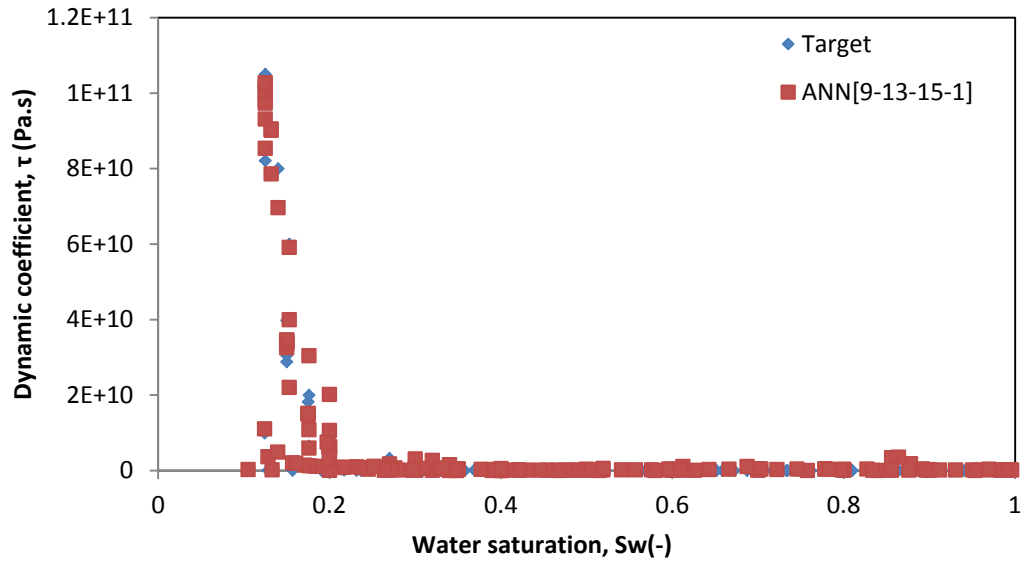

419

420 Figure 7: Plots of the dynamic coefficient values from ANN structures output and target data
421 against water saturation using ANN [9-13-15-1].

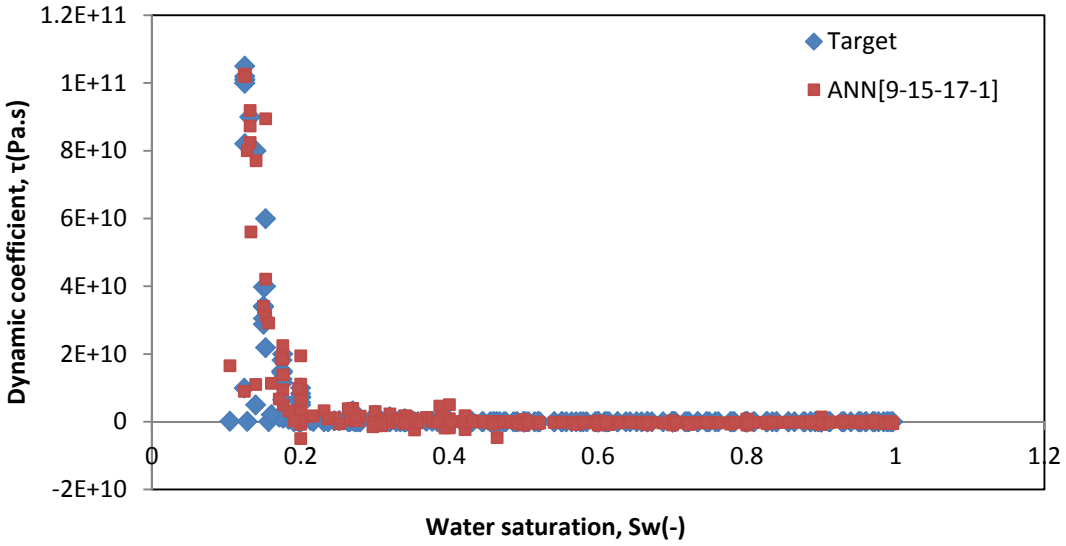

422

423 Figure 8: Plots of the dynamic coefficient values from ANN structures output and target data
424 against water saturation using ANN [9-15-17-1].

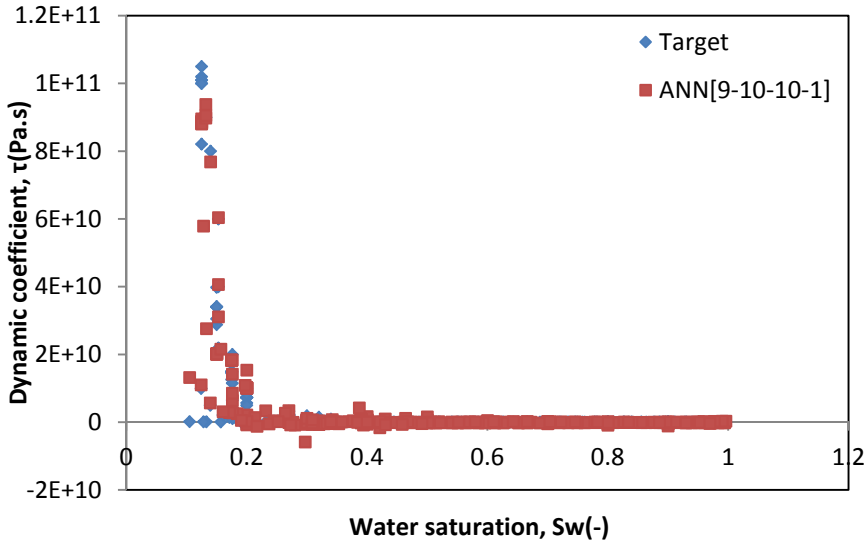

425

426 Figure 9: Plots of the dynamic coefficient values from ANN structures output and target data
427 against water saturation using ANN [9-10-10-1].

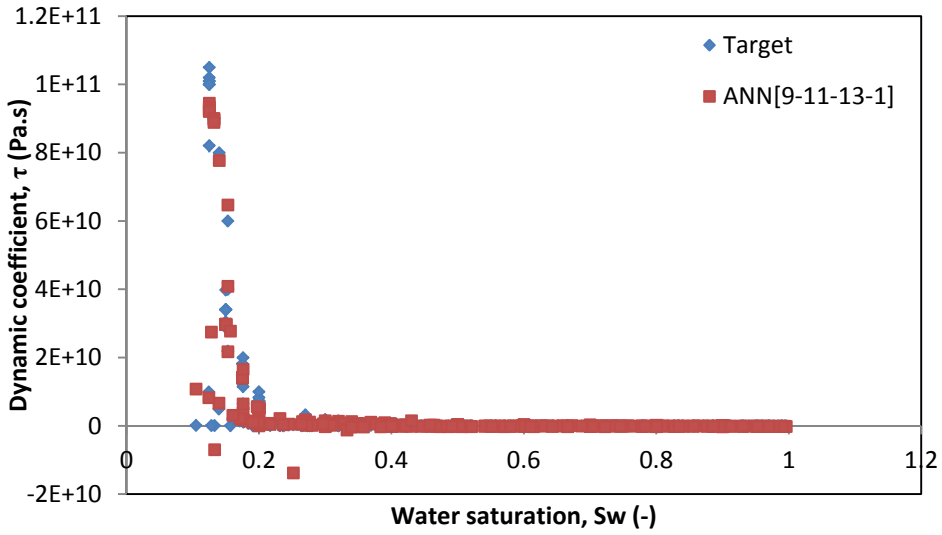

428

429 Figure 10: Plots of the dynamic coefficient values from ANN structures output and target
430 data against water saturation using ANN [9-11-13-1].

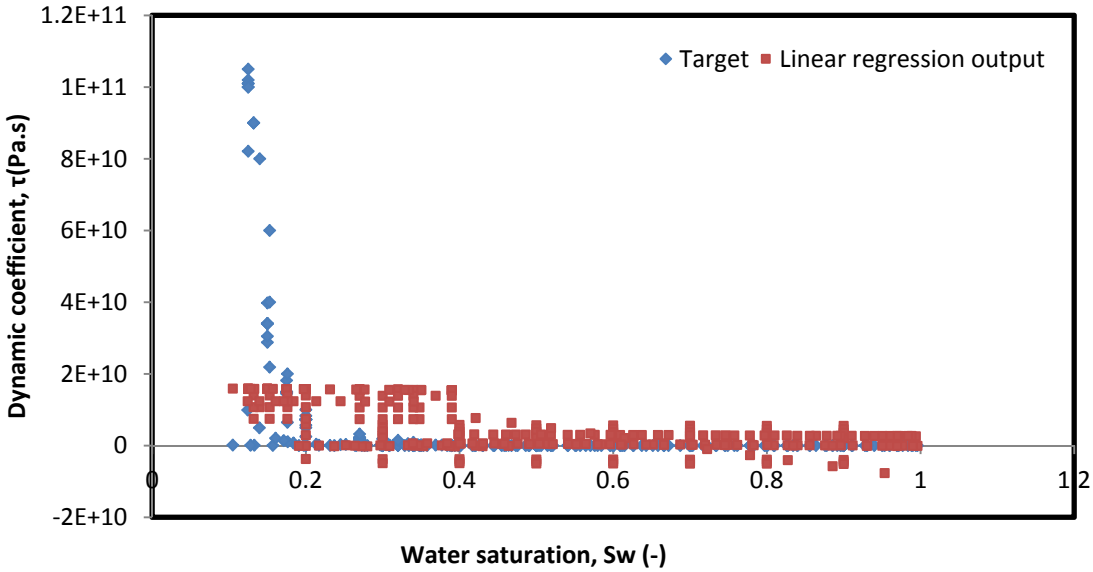

431

432 Figure 11: Plots of the dynamic coefficient against the water saturation values for the entire
433 dataset and the predictions by linear regressions structure.

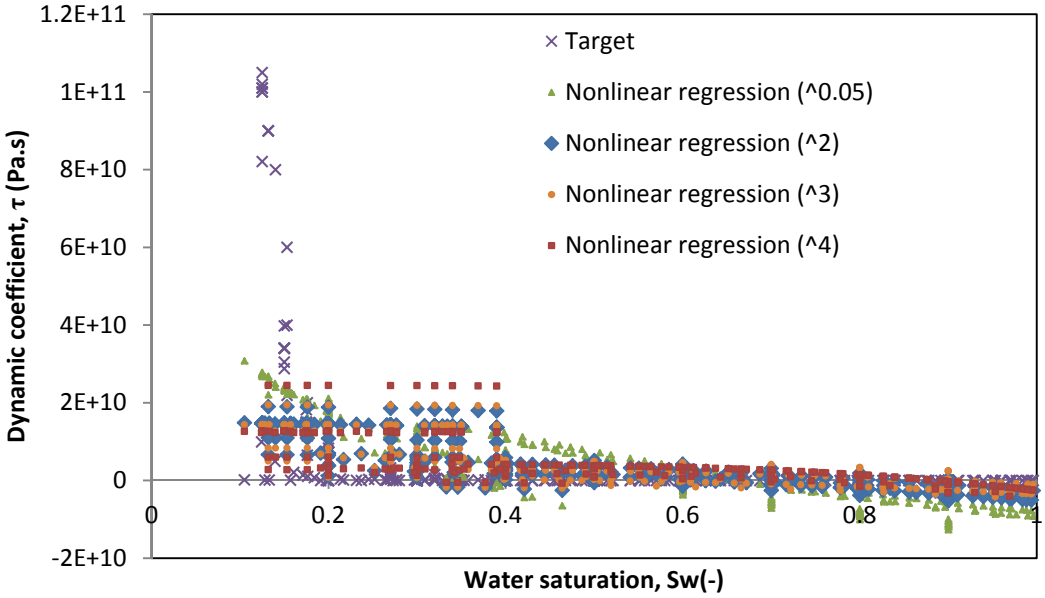

434
435 Figure 12: Plots of the dynamic coefficient against the water saturation values for the entire
436 dataset and the predictions by non-linear regression structures

437

438

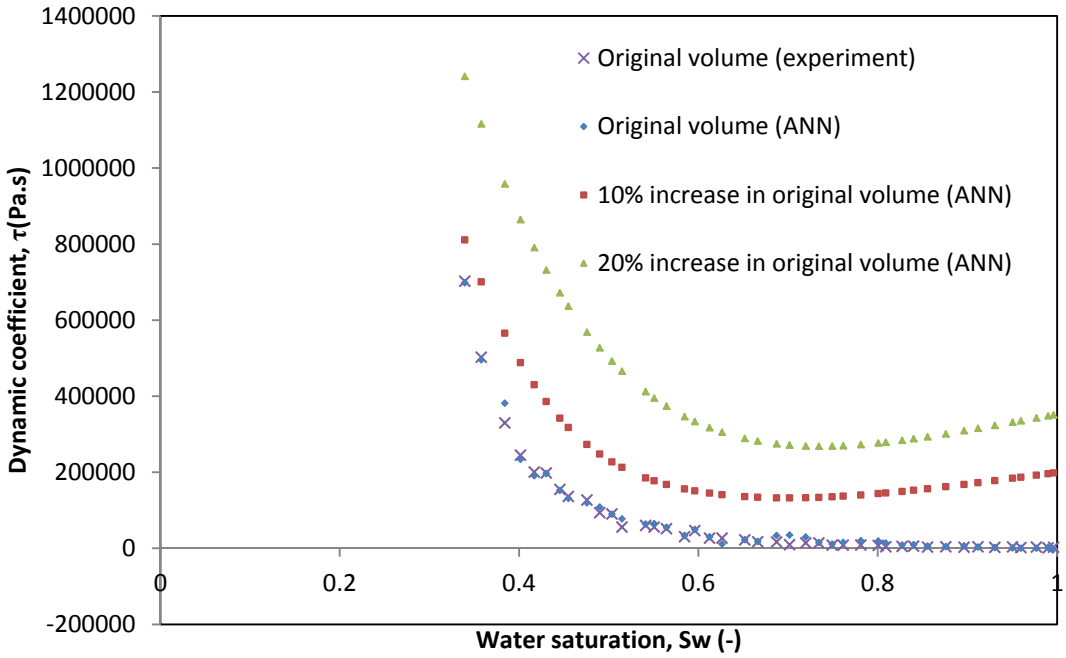

439

440 Figure 13: Prediction of dynamic coefficient values against water saturation for the original,
441 10%, and 20% increase in domain size using the ANN [9-13-15-1]. Data for the original
442 domain size were obtained from Das and Mirzaei (2012) where the oil viscosity is 200 cSt.

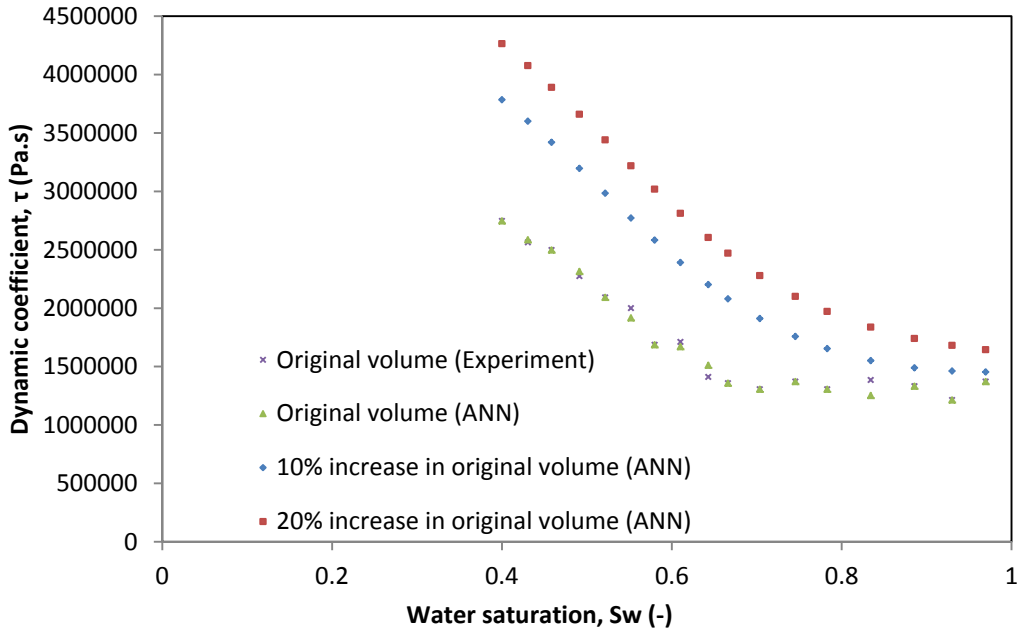

443

444 Figure 14: Prediction of dynamic coefficient values against water saturation for the original,
445 10%, and 20% increase in domain size using ANN [9-13-15-1]. Data for original domain size
446 were obtained from Goel and O'Carroll (2011) where the oil viscosity is 5 cSt.

This trend points to an important observation in the literature about the τ-S dependency on the domain scale. A number of authors have reported the same phenomenon (Bottero et al. 2011; Dahle et al. 2005). Bottero et al.(2011) found that there is a shift to higher values in the τ-S relationships as the scale goes from local measurements to higher averaging windows. Also, Dahle et al. (2005) using a bundle of tubes model reports this phenomenon with a greater effect of scale on τ-S relationships which is said to be proportional to the square of the length of the domain.

Furthermore, using the experimental results by Goel and O'Carroll (2011), increasing the domain volume shows increase in the τ-S relationships. This is shown in Figure 14. The relationship for 10% increases in the domain size lies above the τ-S curve from the original experimental domain size. 20% increase in the domain size also shows further rise in the τ-S relationships.

Finally, results from our laboratory for higher viscosity ratio silicone oil-water system (500) were also tested using the ANN [9-13-15-1]. This is shown in Figure 15. It can be seen from the figure that the τ-S curve rises as the domain size increases. But the rise in this case is rather sluggish, especially at higher water saturation. This can be attributed to high viscosity ratio (500) in this case. The original τ-S curve of Das and Mirzaei (2013) shown in Figure 13 uses viscosity ratio of 200 and the work of Goel and O'Carroll (2011) uses viscosity ratio of 5. Viscosity ratio refers to the ratio of the viscosity of the oil to that of the water.

As demonstrated above, the trend in τ-S as the domain size increases, which indicates the dependency of the dynamic effects in the system properties of two-phase flow system on the media characteristics. Since increase in τ indicates increased deviation from equilibrium (Das et al. 2007)**,** the domain size certainly impacts the dynamic P^c-S relationships in two-phase flow in the porous media. Judging from equation (1), increasing the magnitude of τ implies two things. Provided the value of $P^{c,static}$ remains unaffected by domain scale, then the increase in the value of τ is influenced by increasing value of $P^{c,dyn}$ and/or decreasing value of the $\frac{\partial S}{\partial t}$. Thus, it may be rightly considered that $P^{c,dyn}$ increases as the domain scale increases. Similarly, it is plausible to consider that $\frac{\partial S}{\partial t}$ decreases as the domain scale increases which may be caused by decreasing pressure gradient as the domain height or size increases. While the simultaneous impact of the changes, mentioned above, can cause the observed effects on τ**,** the ratio of their contribution may differ. Bottero et al. (2011) observe that the marginal change in pressure difference ($P^{c,dyn}$- $P^{c,static}$) with upscaled windows of observation is less significant. They attribute the change of τ with domain scale

to the $\frac{\partial S}{\partial t}$, which decreases significantly as the domain size or length increases. Thus, $\frac{\partial S}{\partial t}$ plays significant role in the domain scale dependency of τ.

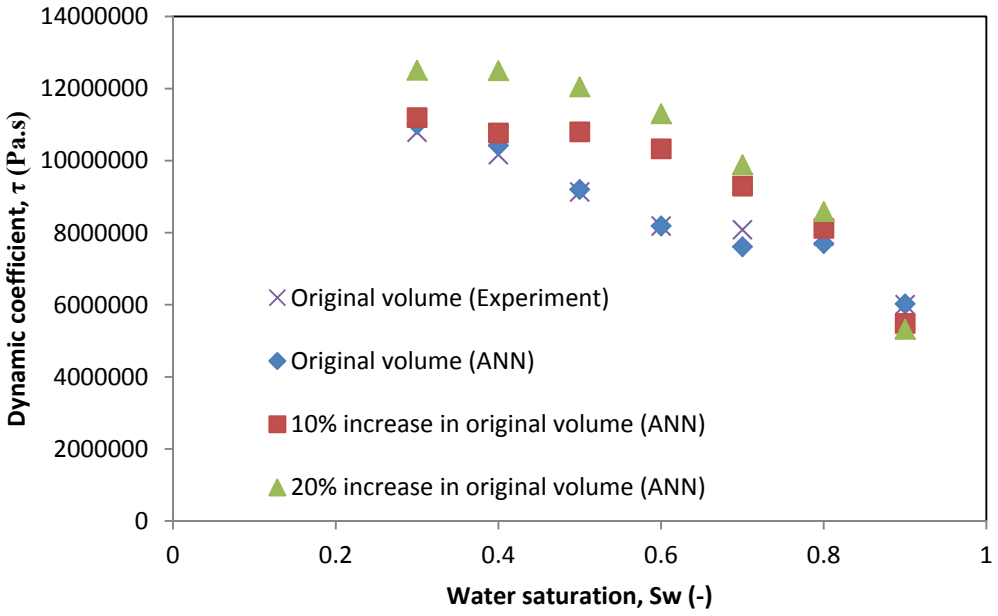

Figure 15: Dynamic coefficient values against water saturation for the original, 10% and 20% increase in domain size using ANN [9-13-15-1]. Data for original domain size were obtained from our laboratory experiments (Abidoye and Das 2014) using methodology described by Mirzaei and Das (2012) but using an oil viscosity of 500 cSt.

4 Conclusion

Application of ANN for the prediction of the scale dependence of the dynamic capillary pressure effects in two-phase flow in porous media has been elaborately demonstrated.

Statistical analyses of the models tested showed that ANN configurations with two-hidden layers outperformed those with single layers. Further comparison of the ANNs with linear and non-linear regression models showed that ANNs have better prediction ability of the two-phase flow system characteristics.

Using the best-performing ANN structure (ANN [9-13-15-1]) in this work, the prediction of the domain size dependency for τ-S relationships reveals that the τ-S curve rises as the domain size increases in all the viscosity ratios tested. It was pointed out that the rate of change of saturation plays more significant role in the domain scale dependency of τ.

Our findings showed the reliability and applicability of the ANN in characterizing and predicting the complex relationships for two-phase flow in porous media. Since the ANN system can be readily accessed and conveniently set up, it offers savings in cost and computational time in comparison to the flow-physics based simulators.

References

Abidoye, L.K. and Das, D.B., 2014. Scale-dependent dynamic capillary pressure effect for two-phase flow in porous media. Advances in Water Resources. DOI: 10.1016/j.advwatres.2014.09.009 (in press).

Ahmadi, M.A., Ebadi, M., Shokrollahi, M., Javad, S.M., 2013. Evolving artificial neural network and imperialist competitive algorithm for prediction oil flow rate of the reservoir. *Applied Soft Computing*, 13(2), pp.1085–1098.

Amato, F., López, A., Peña-Méndez, E.M., Vaňhara, P., Hampl, A., Havel, J., 2013. Artificial neural networks in medical diagnosis. *Journal of Applied Biomedicine*, 11(2), pp.47–58.

Bear, J., 2013. *Dynamics of fluids in porous media*, Courier Dover Publications.

Bottero, S., Hassanizadeh, S.M., Kleingeld, P.J., et al., 2011. Nonequilibrium capillarity effects in two-phase flow through porous media at different scales. *Water Resources Research*, 47(10), p.W10505.

Bottero, S., Hassanizadeh, S.M. and Kleingeld, P.J., 2011. From Local Measurements to an Upscaled Capillary Pressure–Saturation Curve. *Transport in Porous Media*, 88(2), pp.271–291.

Camps-Roach, G. et al., 2010. Experimental investigation of dynamic effects in capillary pressure: Grain size dependency and upscaling. *Water Resources Research*, 46(8), p.W08544.

Dahle, H.K., Celia, M. A. and Hassanizadeh, S.M., 2005. Bundle-of-Tubes Model for Calculating Dynamic Effects in the Capillary-Pressure- Saturation Relationship. *Transport in Porous Media*, 58(1-2), pp.5–22.

Danish, M. and Jacquin, C., 1983. Influence du Contraste des Viscosités sur les Perméabilités Relatives lors du Drainage. Expérimentation et Modélisation. *Rev. Inst. Franc. Pétrole*, 33(6), pp.723–733.

Das, D.B., Gauldie, R. and Mirzaei, M., 2007. Dynamic Effects for Two-Phase Flow in Porous Media : Fluid Property Effects. *AIChE*, 53(10), pp.2505–2520.

Das, D,B., Gill, B.S., Abidoye, L.K. and Khudaida, K.K., 2014. A numerical study of dynamic capillary pressure effect for supercritical carbon dioxide-water flow in porous domain. AIChE journal, DOI: 10.1002/aic.14577 (in press)

Das, D.B. & Mirzaei, M., 2012. Dynamic effects in capillary pressure relationships for two-phase flow in porous media: Experiments and numerical analyses. *AIChE Journal*, 58(12), pp.3891–3903.

Das, D.B. and Mirzaei, M., 2013. Experimental measurement of dynamic effect in capillary pressure relationship for two-phase flow in weakly layered porous media. *AIChE Journal*, 59(5), pp.1723–1734.

Das, D.B., Mirzaei, M. and Widdows, N., 2006. Non-uniqueness in capillary pressure–saturation–relative permeability relationships for two-phase flow in porous media: Interplay between intensity and distribution of random micro-heterogeneities. *Chemical Engineering Science*, 61(20), pp.6786–6803.

Deka, L., Quddus, M., 2014. Network-level accident-mapping: Distance based pattern matching using artificial neural network. Accident Analysis & Prevention, 65, 105–113. DOI: 10.1016/j.aap.2013.12.001.

Diamantopoulos, E. and Durner, W., 2012. Dynamic Nonequilibrium of Water Flow in Porous Media: A Review. *Vadose Zone Journal*, 11(3).

Dullien, F.A.L., Allsop, H.A., Macdonald, I.F. and Chatzis, I., 1990. Wettability and Immiscible Displacement in Pembina Cardium Sandstone Can. *J.P.T.*, 29(4), pp.63-74.

Gielen, T., Hassanizadeh, S.M., Leijnse, A. and Nordhaug, H.F., 2005. Dynamic effects in multiphase flow: a pore-scale network approach. In *Upscaling multiphase flow in porous media*. Springer, pp. 217–236.

Goel, G. and O'Carroll, D.M., 2011. Experimental investigation of nonequilibrium capillarity effects: Fluid viscosity effects. *Water Resources Research*, 47(9), p.W09507.

Hanspal, N. and Das, D., 2012. Dynamic effects on capillary pressure–Saturation relationships for two-phase porous flow: Implications of temperature. *AIChE Journal*, 58(6), pp.1951–1965.

Hanspal, N.S., Allison B.A., Deka L., Das D.B. , 2013. Artificial neural network (ANN) modeling of dynamic effects on two-phase flow in homogenous porous media. *Journal of Hydroinformatics*, 15(2), p.540.

Hassanizadeh, S.M., Celia, M.A. and Dahle, H.K., 2002. Dynamic effect in the capillary pressure--saturation relationship and its impacts on unsaturated flow. *Vadose Zone Journal*, 1(1), pp.38–57.

Hassanizadeh, S.M. and Gray, W.G., 1993. Thermodynamic basis of capillary pressure in porous media. *Water Resources Research*, 29(10), pp.3389–3405. Available at: http://dx.doi.org/10.1029/93WR01495.

Hill, D.J., Minsker, B.S., Valocchi, A.J., Babovic, V., Keijzer, M., 2007. Upscaling models of solute transport in porous media through genetic programming. *Journal of Hydroinformatics*, 9 (4), pp. 251-266.

Hou, L., Chen, L. and Kibbey, T.C.G., 2012. Dynamic capillary effects in a small-volume unsaturated porous medium: Implications of sensor response and gas pressure gradients for understanding system dependencies. *Water Resources Research*, 48(11), p.W1152.

Ingham, D.B. and Pop, I., 2005. *Transport phenomena in porous media III*, Elsevier.

574 Jain, A. and Indurthy, S., 2003. Comparative Analysis of Event-based Rainfall-runoff
575 Modeling Techniques—Deterministic, Statistical, and Artificial Neural Networks. *Journal*
576 *of Hydrologic Engineering*, 8(2).

577 Jain, A. and Ormsbee, L.E., 2002. Short-term water demand forecast modeling techniques:
578 Conventional methods versus AI. *Journal-American Water Works Association*, 94(7),
579 pp.64–72.

580 Joekar-Niasar, V. and Hassanizadeh, S.M., 2011. Effect of fluids properties on non-
581 equilibrium capillarity effects: Dynamic pore-network modeling. *International Journal of*
582 *Multiphase Flow*, 37(2), pp.198–214.

583 Johnson, V.M. and Rogers, L.L., 2000. Accuracy of neural network approximators in
584 simulation-optimization. *Journal of Water Resources Planning and Management*,
585 126(2), pp.48–56.

586 Kalaydjian, F., 1987. A Macroscopic Description of Multiphase Flow in Porous Media
587 involving Space-time Evolution of Fluid/Fluid Interface. *Transport in Porous Media*, 6(2),
588 pp.537–552.

589 Kalaydjian, F., 1992. Effect of the Flow Rate on an Imbibtion Capillary Pressure Curve-
590 Theory Versus Experiment. In *SCA European Core Analysis Symposium, Paris,*
591 *France*.

592 Kalogirou, S.A., 2013. Applications of artificial neural-networks for. *Energy Systems:*
593 *Adaptive Complexity*, p.17.

594 Kalogirou, S.A., 2000. Applications of artificial neural-networks for energy systems. *Applied*
595 *Energy*, 67(1-2), pp.17–35.

596 Karimpouli, S., Fathianpour, N. and Roohi, J., 2010. A new approach to improve neural
597 networks' algorithm in permeability prediction of petroleum reservoirs using supervised
598 committee machine neural network (SCMNN). *Journal of Petroleum Science and*
599 *Engineering*, 73(3), pp.227–232.

600 Khashei, M. and Bijari, M., 2013. Fuzzy artificial neural network (p, d, q) model for
601 incomplete financial time series forecasting. *Journal of Intelligent and Fuzzy Systems*.

602 Khudaida KJ, Das DB, 2014. A numerical study of capillary pressure–saturation relationship
603 for supercritical carbon dioxide (CO_2) injection in deep saline aquifer. Chem Eng Res
604 Des, DOI:10.1016/j.cherd.2014.04.020 (in press)

605 Kobayashi, K., Hinkelmann, R., Helmig, R., 2008.
606 Development of a simulation-optimization model for multiphase systems in the
607 subsurface: A challenge to real-world simulation-optimization,
608 *Journal of Hydroinformatics*, 10 (2), pp. 139-152.

609 Manthey, S., Majid Hassanizadeh, S. and Helmig, R., 2005. Macro-Scale Dynamic Effects in
610 Homogeneous and Heterogeneous Porous Media. *Transport in Porous Media*, 58(1-2),
611 pp.121–145.

612 Marquardt, D.W., 1963. An algorithm for least-squares estimation of nonlinear parameters.
613 *Journal of the Society for Industrial & Applied Mathematics*, 11(2), pp.431–441.

614 Mehta, H.B., Pujara, M.P. and Banerjee, J., 2013. Prediction of Two Phase Flow Pattern
615 Using Artificial Neural Network. In *International Conference on Chemical and*
616 *Environmental Engineering (ICCEE'2013) April 15-16, 2013 Johannesburg (South*
617 *Africa)*.

618 Mirzaei, M. and Das, D.B., 2007. Dynamic effects in capillary pressure–saturations
619 relationships for two-phase flow in 3D porous media: Implications of micro-
620 heterogeneities. *Chemical Engineering Science*, 62(7), pp.1927–1947.

621 Mounce, S.R., Mounce, R. B., Jackson, T., Austin, J., and Boxall, J. B., 2013. Pattern
622 matching and associative artificial neural networks for water distribution system time
623 series data analysis. Journal of Hydroinformatics. doi:10.2166/hydro.2013.057

624 Mueller, A. V and Hemond, H.F., 2013. Extended artificial neural networks: Incorporation of
625 a priori chemical knowledge enables use of ion selective electrodes for in-situ
626 measurement of ions at environmentally relevant levels. *Talanta*, 117, pp.112–118.
627 DOI: 10.1016/j.talanta.2013.08.045

628 O'Carroll, D.M., Abriola, L.M., Polityka, C.A., Bradford, SA, Demond, A.H. , 2005. Prediction
629 of two-phase capillary pressure--saturation relationships in fractional wettability
630 systems. *Journal of contaminant hydrology*, 77(4), pp.247–270.

631 O'Carroll, D.M., Phelan, T.J. and Abriola, L.M., 2005. Exploring dynamic effects in capillary
632 pressure in multistep outflow experiments. *Water Resour. Res.*, 41(11), p.W11419.

633 Oung, O., Hassanizadeh, S.M. and Bezuijen, A., 2005. Two-Phase Flow Experiments in a
634 Geocentrifuge and the Significance of Dynamic Capillary Pressure Effect. *Journal of*
635 *Porous Media*, 8(3), pp.247–257.

636 Rogers, L.L. and Dowla, F.U., 1994. Optimization of groundwater remediation using artificial
637 neural networks with parallel solute transport modeling. *Water Resources Research*,
638 30(2), pp.457–481.

639 S. R. Mounce, R. B. Mounce, T. Jackson, J.A. and J.B.B., 2013. Pattern matching and
640 associative artificial neural networks for water distribution system time series data
641 analysis. *ournal of Hydroinformatics*.

642 Sakaki, T., O'Carroll, D.M. and Illangasekare, T.H., 2010. Direct Quantification of Dynamic
643 Effects in Capillary Pressure for Drainage–Wetting Cycles. *Vadose Zone Journal*, 9(2),
644 p.424.

645 Smiles, D.E., Vachaud, G. and Vauclin, M., 1971. A test of the uniqueness of the soil
646 moisture characteristic during transient, nonhysteretic flow of water in a rigid soil. *Soil*
647 *Science Society of America Journal*, 35(4), pp.534–539.

648 Spalding, D.B., 1981. A general purpose computer program for multi-dimensional one-and
649 two-phase flow. *Mathematics and Computers in Simulation*, 23(3), pp.267–276.

650 Srinivasulu, S. and Jain, A., 2006. A comparative analysis of training methods for artificial
651 neural network rainfall--runoff models. *Applied Soft Computing*, 6(3), pp.295–306.

652 Stauffer, 1978. Time Dependence of the Relations between Capillary Pressure, Water
653 Content and Conductivity During Drainage of Porous Media. In *paper presented at*
654 *IAHR Symp. on Scale Effects in Porous Media*. pp. 766–776.

655 El Tabach, E., Lancelot, L., Shahrour, I., Najjar, Y., 2007. Use of artificial neural network
656 simulation metamodelling to assess groundwater contamination in a road project.
657 *Mathematical and Computer Modelling*, 45(7), pp.766–776.

658 Tian , S. Lei, G., He, S., Yang, L. , 2012. Dynamic effect of capillary pressure in low
659 permeability reservoirs. *Petroleum Exploration and Development*, 39(3), pp.405–411.

660 Topp, G.C., Klute, A. and Peters, D.B., 1967. Comparison of water content-pressure head
661 data obtained by equilibrium, steady-state, and unsteady-state methods. *Soil Science*
662 *Society of America Journal*, 31(3), pp.312–314.

663 Wang, L. & Fu, K., 2008. *Artificial neural networks*, Wiley Online Library.

664 Wildenschild, D., Hopmans, J.W. and Simunek, J., 2001. Flow rate dependence of soil
665 hydraulic characteristics. *Soil Science Society of America Journal*, 65(1), pp.35–48.

666 Yan, S. and Minsker, B., 2006. Optimal groundwater remediation design using an Adaptive
667 Neural Network Genetic Algorithm. *Water Resources Research*, 42(5), DOI:
668 10.1029/2005WR004303.

669 Yurdakul, M. and Akdas, H., 2013. Modeling uniaxial compressive strength of building
670 stones using non-destructive test results as neural networks input parameters.
671 *Construction and Building Materials*, 47, pp.1010–1019.

672 Zhang, G., Eddy Patuwo, B. and Y. Hu, M., 1998. Forecasting with artificial neural networks:
673 *International Journal of Forecasting*, 14(1), pp.35–62.

674